Measurements of the $K\alpha$ transition energies of heliumlike krypton

K. Widmann,* P. Beiersdorfer, and V. Decaux
Lawrence Livermore National Laboratory, California 94551

M. Bitter
Princeton Plasma Physics Laboratory, Princeton, New Jersey 08543

(Received 21 March 1995; revised manuscript received 11 December 1995)

Measurements of the $1s2p^1P_1 \rightarrow 1s^2\,^1S_0$, $1s2p^3P_2 \rightarrow 1s^2\,^1S_0$, $1s2p^3P_1 \rightarrow 1s^2\,^1S_0$, and $1s2s^3S_1 \rightarrow 1s^2\,^1S_0$ transitions in heliumlike krypton (Kr^{34+}) have been made on the Electron Beam Ion Trap (EBIT) facility at the Lawrence Livermore National Laboratory. The measurements were performed using a high-resolution crystal spectrometer and an accuracy of about 30 ppm was achieved. Unlike earlier measurements, our results are in good agreement with recent theoretical predictions.

PACS number(s): 32.30.Rj, 31.30.Jv, 12.20.Fv

I. INTRODUCTION

Spectra of heliumlike ions have been a subject of intense research interest, since these ions are the simplest of all multielectron systems and therefore provide an ideal setting for testing approaches to solve the many-body problem. Although the predictions for the $K\alpha$ transitions of two-electron systems have become very accurate during recent years, there are still significant differences among the theoretical values, depending on the approaches used to account for the many-body quantum-electrodynamical and relativistic corrections as well as electron-electron correlations. Thus experimental results are necessary in order to guide the development of accurate theoretical approximations. This is especially important for high-Z heliumlike ions, as differences among predictions tend to increase strongly with atomic number [1–3]. In the case of krypton, for example, Drake [1] calculates 13 114.33 eV for the $1s2p^1P_1 \rightarrow 1s^2\,^1S_0$ transition using the unified method, which combines high-precision nonrelativistic variational calculations with relativistic and quantum electrodynamic (QED) corrections. However, Plante, Johnson, and Sapirstein [2] predict 13 114.41 eV for the same $n=2 \rightarrow 1$ transition in heliumlike krypton using an iterative method for determining the eigenvalues of the no-pair Hamiltonian, treating the instantaneous Breit interaction as a perturbation, and taking the corrections for mass polarization and QED from Drake [1]. Another prediction made by Cheng, Chen, Johnson, and Sapirstein [3] gives 13 114.70 eV for the $1s2p^1P_1 \rightarrow 1s^2\,^1S_0$ transition in Kr^{34+}. Cheng *et al.* are using a large-scale relativistic configuration interaction calculation obtaining results that are very close to the Dirac energies computed by Plante *et al.* The main difference between the two theoretical values is due to the different ways to account for the QED contributions.

Heliumlike $K\alpha$ radiation has been studied for ions as heavy as Xe^{52+} [4] and U^{90+} [5], but only up to Kr^{34+} with high-resolution crystal spectrometers [6,7]. The experimental results of Briand *et al.* [6] for the krypton $K\alpha$ transitions obtained at the UNILAC accelerator facility are not accurate enough (90–170 ppm) to distinguish between any of the recent theoretical predictions. The values for krypton obtained at the GANIL accelerator facility by Indelicato *et al.* [7] with an accuracy of 0.30 eV (24 ppm) differ significantly from all recent calculations. For the $1s2p^1P_1 \rightarrow 1s^2\,^1S_0$ transition the difference is (0.75 ± 0.30) eV, comparing with the results of the calculations of Cheng *et al.* [3], and (1.12 ± 0.30) eV, comparing with the values calculated by Drake [1]. Thus there is a strong interest in remeasuring the energies of the krypton $K\alpha$ transitions. Our measurement was performed at the Electron Beam Ion Trap (EBIT) facility [8] also using high-resolution crystal spectroscopy [9], and achieving a precision of 28–31 ppm. Unlike earlier measurements at the GANIL accelerator facility [7], the results of our measurement are in agreement with most recent calculations, agreeing best with the values predicted by Cheng, Chen, Johnson, and Sapirstein [3].

II. EXPERIMENT

In EBIT, electron-ion interactions take place along a 2-cm-long region within the 60-μm-diam electron beam [10], making EBIT a perfect line source, which can be imaged by a spectrometer without applying an additional entrance slit. An aperture in the liquid helium shield constrains the accessible height of the EBIT source to 1.2 cm. The measurements were made with a von Hámos–type [11] high-resolution crystal spectrometer using a cylindrically bent 200-LiF crystal ($2d = 4.027$ Å) with a radius of curvature $R = 75$ cm. Figure 1 shows an outline of this setup. The spectrometer is set to a nominal Bragg angle $\theta = 28°$. This setup measures the krypton Kα radiation in second order and the Ly-$\alpha_{1,2}$ lines of manganese as well as the transitions $1s2s^3S_1 \rightarrow 1s^2\,^1S_0$ and $1s2s^22p^1P_1 \rightarrow 1s^22s^2\,^1S_0$ in heliumlike and berylliumlike iron used for calibration in first-order Bragg reflection. The detector, a position sensitive proportional counter, was optimized for the energy range of the He-like krypton K-shell x rays [12]. Aiming for a high quantum efficiency while maintaining good spatial resolution led to the following operating parameters for the detector: gas mixture 70% Xe, 30% CH_4; gas pressure 78 psi (gauge)

*Also at Institut für Experimentalphysik, Technische Universität Graz, Austria.

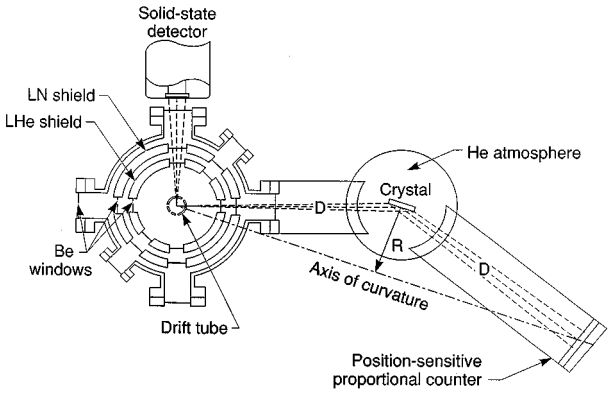

FIG. 1. Layout of the von Hámos spectrometer in the horizontal plane of EBIT. The electron beam is out of the page.

(5.38 bar); active volume $9.5\times3.0\times0.4\text{cm}^3$; thickness of Be window 1 mm; applied voltage 4.2 kV. We obtained an efficiency of about 70% for first-order x-ray photons (6.5 keV) and about 55% for the second-order krypton K-shell x rays (13 keV), taking into account the absorption due to the Be windows in EBIT and the detector, respectively. The difference in the efficiency is mainly due to the different mean ionization depths for these photon energies in the detector. The influence of this difference on the determination of the transition energies will be discussed in Sec. III. A spatial resolution of $\Delta x_{\text{detector}}=80-100$ μm was achieved along the whole detector area. This was measured with an ^{55}Fe x-ray source ($E_{\text{x rays}}\approx6$ keV), and a Rb $K\alpha$ source ($E_{\text{x rays}}\approx14$ keV), respectively.

The spatial resolution is only one of several factors which limit the resolving power of the spectrometer. Further decrease of the resolving power of this setup is caused by the finite size of the source, the imaging properties of the von Hámos geometry, the resolving power of the LiF crystal, and thermal line broadening. The size of the source is given by the diameter of the electron beam, which is $\Delta x_{\text{beam}}=60$ μm [10]. Calculating the imaging properties of the von Hámos geometry [11] gives a line spread of less than $\Delta x_{\text{image}}=30$ μm. Accounting only for geometrical effects, i.e., spatial resolution of the detector, beamwidth, and imaging properties, the highest achievable resolving power of our setup would be $(E/\Delta E)_{\text{geom}}=14\,000-16\,500$. The difference to the measured resolution of $E/\Delta E\approx2600$ for Fe^{24+} and Mn^{24+} in first, and $E/\Delta E\approx4300$ for Kr^{34+} in second, order shows that thermal line broadening and the resolving power of the crystal are the main contributions to the limitation of the resolving power. For the lines emitted by the highly charged ions in EBIT, Doppler broadening is the dominant broadening process. The linewidth [full width at half maximum (FWHM)] due to the Doppler broadening can be calculated using the equation

$$\Delta E=E\sqrt{\frac{8\ln(2)T_{\text{ion}}}{m_{\text{ion}}c^2}}. \tag{1}$$

T_{ion} is the temperature and m_{ion} the mass of the ion, E the energy of the spectral line, and ΔE the full width of the line at half maximum. At run conditions of EBIT optimized towards the highest intensity of x-ray emission, such as those used in the present measurement where a deep trap ($V_{\text{axial}}=205$ V) and a high beam current ($I_{\text{beam}}=180-200$ mA) have been applied, the temperature of the trapped ions is on the order of 700 eV, as shown earlier in the case of heliumlike Ti^{20+} ions [13,14]. The corresponding Doppler broadening (FWHM) is about $\Delta E_{T_{\text{ion}}}=1.8$ eV for the heliumlike Fe^{24+} and the hydrogenlike Mn^{24+} lines, and about $\Delta E_{T_{\text{ion}}}=2.9$ eV for the heliumlike Kr^{34+} lines. The linewidths in the recorded spectra are $\Delta E_{\text{expt}}=(2.5\pm0.1)$ eV for the hydrogenlike Mn^{24+} and the heliumlike Fe^{24+} lines and $\Delta E_{\text{expt}}=(3.05\pm0.05)$ eV for the heliumlike Kr^{34+} lines. The width of the krypton lines is thus in good agreement with the expected ion temperature. This indicates that in second-order Bragg reflection the resolving power is limited by the Doppler broadening, and the line profile is dominated by the thermal Doppler effect. In first-order Bragg reflection, by contrast, the factor limiting the resolving power appears to be the resolving power of the crystal. In other words, the shape of the spectral lines recorded in first order is dominated by the rocking curve of the crystal [15]. The impact of the different line shapes in first and second order on the measured transition energies will be discussed in Sec. III.

For the observation of the krypton spectra neutral krypton atoms are injected into EBIT by means of a gas injector. The pressure in the gas injector is in the 10^{-8}-Torr range, which is more than three orders of magnitude higher than in the trap itself. Precise adjustment of the gas injector ensures that the krypton atoms hit the electron beam, where they get ionized and trapped. The ionization balance is optimized by choosing an appropriate electron beam energy, trap depth, cooling gas pressure, and the time during which the ions are kept in the trap before they are dumped and the trap is filled up with ''new'' ions [16]. Without the process of dumping and refilling, the background, due to high-Z elements (such as barium and tungsten from the electron filament) getting into the trap, would increase in time.

Introduction of manganese and iron into EBIT for calibration was accomplished by using a metal vapor vacuum arc (MEVVA) [17]. In particular, a MEVVA was constructed with a cathode made from manganese and an iron trigger wire. In normal operation the MEVVA plasma contains mostly atoms and ions from the cathode material, which is Mn. Interchanging the electrical leads between cathode and trigger allows us to inject Fe. Using this MEVVA calibration, measurements of iron and manganese x rays were made successively. By contrast, the trap can be filled with krypton and iron or manganese simultaneously. Thus a krypton spectrum could be recorded simultaneously with a calibration spectrum.

III. MEASUREMENTS

The EBIT facility uses a monoenergetic electron beam for the excitation of the ions. Unlike in plasma observations, this enables us to record spectra produced solely by direct excitation (DE) and without the presence of satellite lines produced by dielectronic recombination. Therefore none of the heliumlike or hydrogenlike lines discussed overlap or blend with satellite transitions from lower charge states. For collecting the krypton data we used an electron beam energy of

about 19.5 keV, well above the excitation threshold for the heliumlike krypton $K\alpha$ transitions, which is around 13 keV. For the manganese calibration the beam energy was set to about 12 keV, which is much higher than the ionization energy of heliumlike manganese ($E_{\rm ion}=8.14$ keV), and yielded the highest count rate for the Ly-α emission. The iron data were collected at a 9-keV electron beam energy, which again is more than necessary for the production of heliumlike iron, i.e., ionization of lithiumlike iron ions ($E_{\rm ion}=2.05$ keV).

Figure 2 shows the heliumlike krypton K-shell spectrum together with the two calibration spectra featuring the manganese Ly-$\alpha_{1,2}$ lines and the $1s2s\ ^3S_1\rightarrow 1s^2\ ^1S_0$, labeled z, and $1s2s^22p^1P_1\rightarrow 1s^22s^2\ ^1S_0$, labeled β, transitions in heliumlike and berylliumlike iron, respectively. The labeling is according to the notation of Gabriel [18]. Additionally, several collisional satellite lines of lower charge states are seen in the spectra of both Kr and Fe. Some of the lithiumlike and berylliumlike satellites are labeled (r,q,t, and β). The analyzed spectra represent data taken in about 44 h, i.e., overall, 9 h manganese, 5 h iron, 26 h krypton, and 4 h where krypton and iron were collected simultaneously. Taking the complete data set, shown in Fig. 2, a count rate of about 100 counts per hour for the $1s2p^1P_1\rightarrow 1s^2\ ^1S_0$ transition and 45 counts per hour for the $1s2s\ ^3S_1\rightarrow 1s^2\ ^1S_0$ transition in Kr^{34+} can be derived. For the calibration lines the count rate was about 230 counts per hour for the Mn Ly-α_1 line, and 315 counts per hour for the heliumlike iron transition, respectively. For calibration we set the value of the Mn Ly-α_1 line equal to 6441.665 eV, as calculated by Mohr [19] and Johnson and Soff [20], the iron $1s2s^3S_1\rightarrow 1s^2\ ^1S_0$ transition equal to (6636.84±0.39) eV, and the $1s2s^22p^1P_1\rightarrow 1s^22s^2\ ^1S_0$ transition equal to (6628.93 ± 0.29) eV as measured by Beiersdorfer *et al.* [21]. These three lines determine both the absolute energy scale and the spectral dispersion. The iron transitions β and z have been chosen for the calibration because there is no published energy or wavelength measurement of r with sufficient accuracy (in plasma observations r blends with dielectronic satellite transitions). The lines q and y are too close to the edge of the illuminated area of the detector. Using these lines as references would add an unknown systematic uncertainty to the determination of their line centroids. For the same reason we abstained from using the Mn Ly-α_2 line for our calibration.

For the conversion from first- to second-order energies it is necessary to account for parallax effects in the position sensitive detector due to the different mean ionization depth, for the differences in the diffraction images due to the crystal, and for differences in the index of refraction of the crystal. Taking the mass attenuation for Xe, C, and H [22] (detector gas filling: 70% Xe, 30% CH_4; gas pressure 5.38 bar; thickness: 4 mm) a mean ionization depth of $z_{\rm ion}=0.697(2)$ mm for the 6.5-keV x rays and $z_{\rm ion}=1.711(1)$ mm for the 13-keV x rays can be derived. Despite this difference the line shift relative to the krypton lines due to parallax effects is less than 8 μm for the Mn Ly-α_1 lines and less than 7 μm for the Fe $K\alpha$ transitions. For both the manganese and the iron spectra, parallax shifts the lines away from the center of the detector. This spatial shift of the calibration lines changes the energy of the krypton $1s2p^1P_1\rightarrow 1s^2\ ^1S_0$ transition by -0.02 eV and the krypton $1s2s^3S_1\rightarrow 1s^2\ ^1S_0$ transition by $+0.03$ eV. The parallax

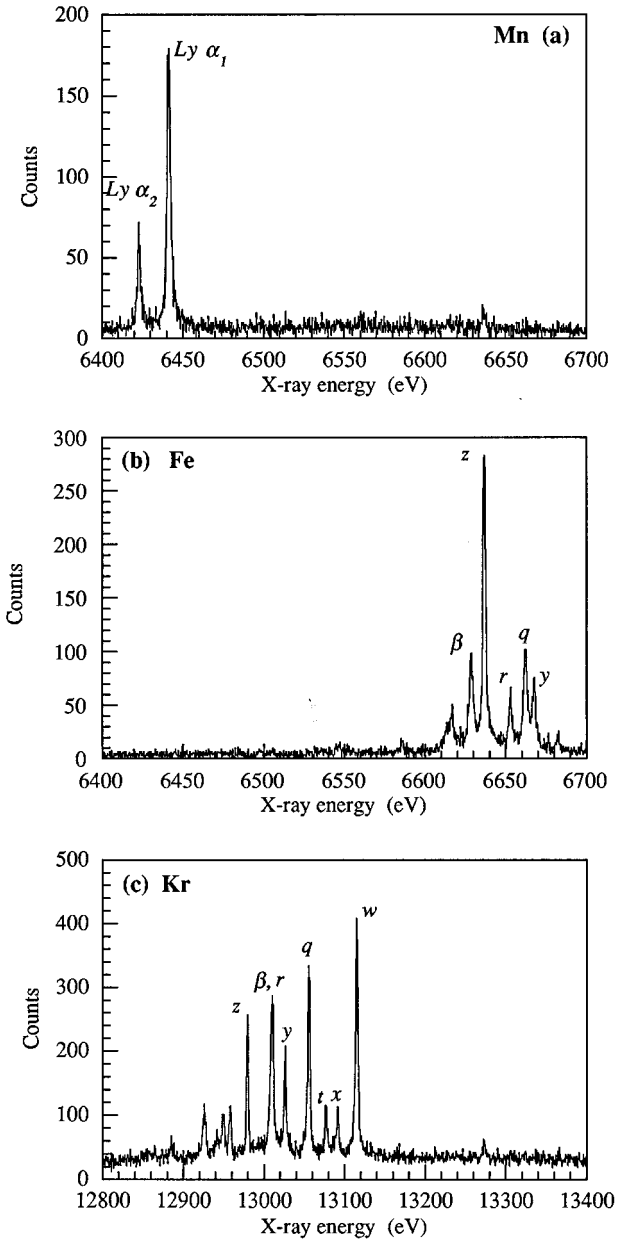

FIG. 2. (a) Spectrum of hydrogenlike manganese showing the Ly-α_1 and Ly-α_2 lines. The electron beam energy was set to 12 keV. (b) Spectrum of the $1s2s^3S_1\rightarrow 1s^2\ ^1S_0$ transition in heliumlike iron, labeled z, recorded at a beam energy of 9 keV. Both the manganese and the iron spectra were taken in first-order Bragg reflection. (c) Krypton $K\alpha$ spectrum measured in second order, setting the electron beam energy to 19.5 keV. In addition to the four He-like transitions (w, x, y, z) both the krypton and iron spectra show collisional satellite lines of lower charge states. Only a few lithiumlike and one berylliumlike satellites of these are labeled (r, q, t, and β).

effects, thus, are small especially when compared to the uncertainties of our measurements discussed below. Adjustments for these effects, however, have been made. The reason for such small effects is the large distance between the source and the detector. Another important issue when using different orders of diffraction is the inter–order comparison of the diffraction images. In our measurements, as already

TABLE I. Experimental and theoretical values for the energies of the $1s2s,1s2p \rightarrow 1s^2$ transitions in heliumlike krypton and average difference between experimental results and the calculated values.

Key	Transition	E_{expt}[a] (eV)	E_{expt}[b] (eV)	E_{theor}[c] (eV)	E_{theor}[d] (eV)	E_{theor}[e] (eV)
w	$1s2p\,^1P_1 \rightarrow 1s^2\,^1S_0$	13114.68(36)	13115.45(30)	13114.33	13114.41	13114.70
x	$1s2p\,^3P_2 \rightarrow 1s^2\,^1S_0$	13091.17(37)		13090.72	13090.79	13091.10[f]
y	$1s2p\,^3P_1 \rightarrow 1s^2\,^1S_0$	13026.29(36)	13026.80(30)	13025.99	13026.05	13026.32
z	$1s2s\,^3S_1 \rightarrow 1s^2\,^1S_0$	12979.63(41)		12979.13	12979.20	12979.51[f]
Average difference:		$\langle E_{\text{expt}}{}^{b} - E_{\text{theor}} \rangle$ (eV)		0.97(30)	0.90(30)	0.60(30)
		$\langle E_{\text{expt}}{}^{a} - E_{\text{theor}} \rangle$ (eV)		0.40(38)	0.33(38)	0.03(38)

[a]Present measurement.
[b]Indelicato *et al.*, Ref. [7].
[c]Drake, Ref. [1].
[d]Plante *et al.*, Ref. [2].
[e]Cheng *et al.*, Ref. [3].
[f]Cheng *et al.*, Ref. [3] and Chen *et al.*, Ref. [28].

mentioned in Sec. II, the line shape for the spectra taken in second-order Bragg reflection is dominated by the Doppler broadening. In contrast, the width of the spectral lines diffracted in first order is limited by the resolving power of the crystal. In fact, the line profile of the spectral lines measured in first-order Bragg reflection is slightly asymmetric. Therefore applying a symmetrical fit function does not give the center of gravity of the spectral line. For example, for the Mn Ly-α_1 line this difference between the center of gravity and the centroid, obtained by using a symmetric fit function, is 0.01 eV. Accounting for this asymmetry of the spectral lines in first order shifts the measured transition energies of the krypton lines on average by 0.02 eV towards lower energies. Conservatively, we assign a 100% uncertainty to this shift. Again, the line shape effects are small compared to the overall uncertainties of our measurements. By contrast, the impact of the difference in the index of refraction on the transition-energy determination is significant. Including the dependence of the index of refraction from the x-ray energy modifies the Bragg equation in the following way [23]:

$$\lambda = \frac{2d_\infty}{n}\left[1 - \frac{\delta}{\lambda^2}\left(\frac{2d_\infty}{n}\right)^2\right]\sin\theta, \tag{2}$$

where d_∞ is the lattice spacing at x-ray energies far above any resonance line of the crystal, n is the order of diffraction, δ the refractivity, i.e., unit decrement of the index of refraction μ, with $\delta = 1-\mu$, λ the wavelength of the x rays in air, and θ the Bragg angle. By comparing Eq. (2) with the Bragg formula,

$$\lambda = \frac{2d_n}{n}\sin\theta, \tag{3}$$

an expression for $2d_n$ can be derived, which includes the dependence on the order of diffraction and the wavelength:

$$2d_n = 2d_\infty\left[1 - \frac{\delta}{\lambda^2}\left(\frac{2d_\infty}{n}\right)^2\right]. \tag{4}$$

The refractivity δ was calculated using an approximation of the dispersion formula for photon energies much higher than the resonance transitions of the medium [24]. Comparison of the inner-shell resonances of lithium, less than 55 eV, and fluorine, less than 686 eV [25], with the x-ray energies being measured (around 6.5 keV in first and 13 keV in second order) justifies this assumption. In this case, the expression for δ, using SI units, is

$$\delta = \frac{N_e\, e^2 \lambda^2}{8\pi^2 \epsilon_0 m_e c^2}. \tag{5}$$

N_e is the electron density in the crystal, e the elementary charge, ϵ_0 the permittivity of vacuum, and m_e the electron rest mass. Thus the expression δ/λ^2 is a constant factor. Taking a lattice spacing of $2d_\infty = 4.027$ Å for the LiF (200) crystal [15] Eq. (4) leads to $2d = 4.026\,78$ Å for first order and $2d = 4.026\,95$ Å for second order. The difference of the index of refraction for the two orders, consequently, has a significant effect on the determination of the energy of second-order lines that are calibrated by lines measured in first order. If neglected, the energies of the second-order lines are 0.54 eV higher than if taken into account. Uncertainties in the determination of $2d_1$ and $2d_2$ arise from the assumed values of $2d_\infty$ and δ/λ^2. An estimate for the uncertainty of the former can be given based on the 0.1-mÅ spread of values cited by different authors [15,26]. A 0.1% change (0.4 mÅ) affects the measured krypton line energies by no more than 0.02 eV. A 10% change in the value of δ/λ^2, which is much higher than expected from basic theoretical considerations [24], affects the measured krypton line energies by only 0.04 eV.

Table I presents the results of the energy determination of the He-like DE lines. The uncertainty in the determination of the transition energies results from the uncertainty of the calibration lines, the uncertainty of the dispersion along the detector, the uncertainty in the determination of the centroid of each line, which includes the uncertainty due to the different line profiles in the first- and second-order spectra, as well as the uncertainty in the assumed values for $2d_1$ and $2d_2$. The uncertainty in the energy of the calibration lines is

TABLE II. Experimental and theoretical values for the QED contributions to the energies of the $1s2s,1s2p \rightarrow 1s^2$ transitions in heliumlike krypton.

Key	Transition	E_{expt}[a] (eV)	$E_{\text{non-QED}}$[b] (eV)	E_{QED}[c] (eV)	E_{QED}[d] (eV)	E_{QED}[a] (eV)
w	$1s2p\,^1P_1 \rightarrow 1s^2\,^1S_0$	13114.68(36)	13125.46(3)	−11.06	−10.73	−10.78(39)
x	$1s2p\,^3P_2 \rightarrow 1s^2\,^1S_0$	13091.17(37)	13101.82(2)	−11.08		−10.65(39)
y	$1s2p\,^3P_1 \rightarrow 1s^2\,^1S_0$	13026.29(36)	13037.19(4)	−11.21	−10.87	−10.90(40)
z	$1s2s\,^3S_1 \rightarrow 1s^2\,^1S_0$	12979.63(41)	12988.74(2)	−9.59		−9.11(43)

[a]Present measurement.
[b]Transition energies without QED contribution, Drake, Cheng *et al.*, and Chen *et al.*, Refs. [1,3,28].
[c]Drake, Ref. [1].
[d]Cheng *et al.*, Ref. [3].

0.4 ppm for the Mn Ly-α_1 line [19,20], 59 ppm for the Fe $1s2s\,^3S_1 \rightarrow 1s^2\,^1S_0$ transition, and 43 ppm for the Fe $1s2s^2 2p\,^1P_1 \rightarrow 1s^2 2s\,^1S_0$ transition [21]. Including the uncertainty of the determination of the centroid of these calibration lines which depends mainly on counting statistics, we get 7 ppm for the Mn Ly-α_1, 59 ppm for the Fe $1s2s\,^3S_1 \rightarrow 1s^2\,^1S_0$ transition, and 44 ppm for the Fe $1s2s^2 2p\,^1P_1 \rightarrow 1s^2 2s\,^1S_0$ transition. As a result, the overall uncertainty of the krypton lines, which includes the uncertainties of the calibration lines, of the dispersion, and of the position of the centroid of the measured lines, ranges from 28 to 31 ppm.

We find (13 114.69 ± 0.36) eV for the $1s2p\,^1P_1 \rightarrow 1s^2\,^1S_0$ transition. This value is 0.76 eV smaller than the (13 115.45 ± 0.30)-eV value measured by Indelicato *et al.* [7]. It remains, however, larger than the 13 114.33-eV value predicted by Drake, in line with the systematic differences noted between Drake and measurements of the $1s2p\,^1P_1 \rightarrow 1s^2\,^1S_0$ transition in various heliumlike ions with $16 \leqslant Z \leqslant 36$ [27]. Nevertheless, within uncertainties, our value is in agreement with all recent calculations [1–3], including Drake's, and in best agreement with the calculation of Cheng, Chen, Johnson, and Sapirstein [3], who predicted 13 114.70 eV. Similarly, our value for the $1s2p\,^3P_1 \rightarrow 1s^2\,^1S_0$ transition of (13 026.29 ± 0.36) eV agrees within uncertainties with all recent calculations and agrees best with the 13 026.36-eV transition energy calculated by Cheng *et al.* [3]. Again, our value is smaller than the (13 026.80 ± 0.30)-eV value determined by Indelicato *et al.* [7].

In addition, we observed the transitions $1s2p\,^3P_2 \rightarrow 1s^2\,^1S_0$, (13 091.17 ± 0.37) eV, and $1s2s\,^3S_1 \rightarrow 1s^2\,^1S_0$, (12 979.63 ± 0.41) eV, in heliumlike krypton. These dipole-forbidden transitions were not observed in the earlier accelerator measurements by Indelicato *et al.* [7]. For both transitions, labeled x and z, the values calculated by Drake, 13 090.72 eV for the $1s2p\,^3P_2 \rightarrow 1s^2\,^1S_0$, and 12 979.13 eV for the $1s2s\,^3S_1 \rightarrow 1s^2\,^1S_0$ transition, are significantly smaller than our measured values. The transition energies predicted by Plante for these lines are 0.01 eV below the $1-\sigma$ uncertainty interval of our measurements. For these two lines there are no values given by Cheng *et al.* [3]. However, by combining earlier results of Chen, Cheng, and Johnson [28] from configuration interaction (CI) calculations of $n=2$ triplet states in heliumlike krypton with the work of Cheng *et al.* [3], the values of 13 091.10 eV for the $1s2p\,^3P_2 \rightarrow 1s^2\,^1S_0$ transition and 12 979.51 eV for the $1s2s\,^3S_1 \rightarrow 1s^2\,^1S_0$ transition can be derived. These values are in excellent agreement with our measurements.

The main difference between the predicted values for the transition energies is due to the different ways of accounting for the QED contributions. Comparing the non-QED part of the calculated values between Drake, Plante *et al.*, Cheng *et al.*, and Chen *et al.* [1–3,28], agreement within 4–6 ppm is found for the $n=2 \rightarrow 1$ transitions in heliumlike krypton. For the $1s2p\,^1P_1 \rightarrow 1s^2\,^1S_0$ transition, for example, the predictions for the transition energy without QED contribution are between 13 125.43 eV (Cheng *et al.*) and 13 125.49 eV (Drake). Thus we find a QED contribution of −10.78(39) eV for the $1s2p\,^1P_1 \rightarrow 1s^2\,^1S_0$ transition by subtracting the non-QED energy of 13 125.46(3) eV from our measured transition energy [13 114.68(36) eV]. Our result agrees best with the −10.73 eV calculated by Cheng *et al.* for the QED contribution to this transition. A comparison between our results of the determination of the QED contribution and the values predicted by theory is presented in Table II. In general, the QED contributions calculated by Drake are larger than measured. The difference is most significant for the $1s2s\,^3S_1 \rightarrow 1s^2\,^1S_0$ transition.

IV. CONCLUSION

The earlier measurement of the heliumlike krypton lines by Indelicato *et al.* [7] was in significant disagreement with the predictions of Drake [1], Plante *et al.* [2], and Cheng *et al.* [3]. The average difference between the values measured by Indelicato *et al.* [7] and the values calculated by Drake [1] is (0.97 ± 0.30) eV, (0.90 ± 0.30) eV comparing with Plante *et al.* [2], and (0.60 ± 0.30) eV comparing with Cheng *et al.* [3]. By contrast, our measurements are in much better agreement with theoretical predictions, as our measurements for the $1s2p\,^1P_1 \rightarrow 1s^2\,^1S_0$ and $1s2p\,^3P_1 \rightarrow 1s^2\,^1S_0$ transition energies are 0.64 eV lower than those measured by Indelicato *et al.* [7]. Like the measurements by Indelicato *et al.*, our measurements differ on average most from those of Drake. Taking the average difference for all four heliumlike transitions we get (0.40 ± 0.38) eV. Comparison with the calculations by Plante *et al.* [2] gives an average difference of (0.33 ± 0.38) eV,

which agrees better with our measurements than the average difference with Drake's calculations. The better agreement appears to reflect the higher accuracy of the calculation by Plante *et al.*, who included new terms in $(Z\alpha)$ for the relativistic energies beyond those included by Drake. Best agreement is found with the theory of Cheng *et al.* [3], where the average difference between our measured values and their predictions is (0.03 ± 0.38) eV. Their calculations match the accuracy of the relativistic energies of Plante *et al.* [2], while including a new approach for estimating the QED contributions. Cheng *et al.* [3] predict 10.68 eV for the QED contribution to the $1s^2\,{}^1S_0$ ground state energy and -0.19 eV for the QED contribution of the $1s2p\,{}^3P_1$ state. Therefore the total QED contribution to the $1s2p\,{}^3P_1\rightarrow 1s^2\,{}^1S_0$ transition should be 10.87 eV. Our result of $E_{\rm QED}=10.90(40)$ eV (see Table II) tests this value to within 4%. Moreover, our measurements are sensitive enough to test the 1.4-eV QED contribution to the energy of the $1s2s$ levels.

The uncertainty of our measurements is too large to be able to distinguish definitively between the predictions made by Plante *et al.* [2] and Cheng *et al.* [3]. For that purpose the uncertainty has to be less than 0.15 eV or 12 ppm. The accuracy of our measurements was limited mainly by the uncertainty of the Fe^{24+} and Fe^{22+} calibration lines (59 and 43 ppm, respectively). As more accurate values for the iron lines become available, the accuracy of our technique will improve and be limited by statistical considerations. Such considerations limit the accuracy of the present measurements to 10–15 ppm.

ACKNOWLEDGMENTS

We thank E. Magee and D. Nelson for their technical support. This work was performed under the auspices of U.S. DOE by Lawrence Livermore National Laboratory under Contract No. W-7405-ENG-48 and supported by the Office of Fusion Energy of the Department of Energy, Division of Applied Plasma Physics.

[1] G.W. Drake, Can. J. Phys. **66**, 586 (1988).
[2] D.R. Plante, W.R. Johnson, and J. Sapirstein, Phys. Rev. A **49**, 3519 (1994).
[3] K.T. Cheng, M.H. Chen, W.R. Johnson, and J. Sapirstein, Phys. Rev. A **50**, 247 (1994).
[4] J.P. Briand, P. Indelicato, A. Simionovici, V. San Vicente, D. Liesen, and D. Dietrich, Europhys. Lett. **9**, 225 (1989).
[5] J.P. Briand, P. Chevallier, P. Indelicato, K.P. Ziock, and D.D. Dietrich, Phys. Rev. Lett. **65**, 2761 (1990).
[6] J.P. Briand, P. Indelicato, M. Tavernier, O. Gorceix, D. Liesen, H.F. Beyer, B. Liu, A. Warczak, and J.P. Desclaux, Z. Phys. A **318**, 1 (1984).
[7] P. Indelicato, J.P. Briand, M. Tavernier, and D. Liesen, Z. Phys. D **2**, 249 (1986).
[8] M.A. Levine, R.E. Marrs, J.R. Henderson, D.A. Knapp, and M.B. Schneider, Phys. Scr. **T22**, 157 (1988).
[9] P. Beiersdorfer, R. Cauble, S. Chantrenne, M. Chen, N. DelGrande, D. Knapp, R. Marrs, A. Osterheld, K. Reed, M. Schneider, J. Scofield, B. Wargelin, K. Wong, D. Vogel, and R. Zasadzinski, in *UV and X-Ray Spectroscopy of Astrophysical and Laboratory Plasmas*, edited by E. Silver and S. Kahn (Cambridge University Press, Cambridge, England, 1993), p. 59.
[10] M.A. Levine, R.E. Marrs, C.L. Bennett, J.R. Henderson, D.A. Knapp, and M.B. Schneider, in *International Symposium on Electron Beam Ion Sources and Their Applications*, edited by A. Hershcovitch, AIP Conf. Proc. No. 188 (AIP, New York, 1989), p. 82.
[11] L. von Hámos, Ann. Phys. (Leipzig) **17**, 716 (1933).
[12] D. Vogel, P. Beiersdorfer, V. Decaux, and K. Widmann, Rev. Sci. Instrum. **66**, 776 (1995).
[13] P. Beiersdorfer, V. Decaux, S. Elliott, K. Widmann, and K. Wong, Rev. Sci. Instrum. **66**, 303 (1995).
[14] P. Beiersdorfer, V. Decaux, and K. Widmann, Nucl. Instrum. Methods Phys. Res. B **98**, 566 (1995).
[15] A. Burek, Space Sci. Instrum. **2**, 53 (1976).
[16] R.E. Marrs, C. Bennett, M.H. Chen, T. Cowan, D. Dietrich, J.R. Henderson, D.A. Knapp, M.A. Levine, K.J. Reed, M.B. Schneider, and J.H. Scofield, J. Phys. (Paris) Colloq. **50**, C1-445 (1989).
[17] I.G. Brown, J.E. Galvin, R.A. MacGill, and R.T. Wright, Appl. Phys. Lett. **49**, 1019 (1986).
[18] A.H. Gabriel, Mon. Not. R. Astron. Soc. **160**, 99 (1972).
[19] P.J. Mohr, At. Data Nucl. Data Tables **29**, 453 (1983).
[20] W.R. Johnson and G. Soff, At. Data Nucl. Data Tables **33**, 405 (1985).
[21] P. Beiersdorfer, T. Phillips, V.L. Jacobs, K.W. Hill, M. Bitter, S. von Goeler, and S.M. Kahn, Astrophys. J. **409**, 846 (1993).
[22] J.W. Robinson, *Handbook of Spectroscopy* (CRC Press, Inc., Cleveland, 1974), Vol. I, p. 28ff.
[23] A.H. Compton and S.K. Allison, *X-Rays in Theory and Experiment* 2nd ed. (Van Nostrand, Princeton, 1935), p. 674.
[24] A.H. Compton and S.K. Allison, *X-Rays in Theory and Experiment*, (Ref. [23]), p. 280.
[25] *CRC Handbook of Chemistry and Physics*, 68th ed. (CRC Press, Inc., Boca Raton, FL, 1987), p. E-181.
[26] N.G. Alexandropoulos and G.G. Cohen, Appl. Spectrosc. **28**, 155 (1974).
[27] P. Beiersdorfer, M. Bitter, S. von Goeler, and K.W. Hill, Phys. Rev. A **40**, 150 (1989).
[28] M.H. Chen, K.T. Cheng, and W.R. Johnson, Phys. Rev. A **47**, 3692 (1993).